STRUCTURAL BIOLOGY

eIF2B-catalyzed nucleotide exchange and phosphoregulation by the integrated stress response

Lillian R. Kenner[1]*, Aditya A. Anand[1,2]*, Henry C. Nguyen[1], Alexander G. Myasnikov[1,3], Carolin J. Klose[1,2], Lea A. McGeever[1,2], Jordan C. Tsai[1,2], Lakshmi E. Miller-Vedam[1], Peter Walter[1,2]†, Adam Frost[1,4]†

The integrated stress response (ISR) tunes the rate of protein synthesis. Control is exerted by phosphorylation of the general translation initiation factor eIF2. eIF2 is a guanosine triphosphatase that becomes activated by eIF2B, a two-fold symmetric and heterodecameric complex that functions as eIF2's dedicated nucleotide exchange factor. Phosphorylation converts eIF2 from a substrate into an inhibitor of eIF2B. We report cryo–electron microscopy structures of eIF2 bound to eIF2B in the dephosphorylated state. The structures reveal that the eIF2B decamer is a static platform upon which one or two flexible eIF2 trimers bind and align with eIF2B's bipartite catalytic centers to catalyze nucleotide exchange. Phosphorylation refolds eIF2α, allowing it to contact eIF2B at a different interface and, we surmise, thereby sequestering it into a nonproductive complex.

Numerous factors regulate translation of the genetic code into proteins, including eukaryotic translation initiation factor 2 (eIF2), a guanosine triphosphatase (GTPase) composed of α, β, and γ subunits. During initiation, eIF2 binds $tRNA^{Met}$ and GTP to form a ternary complex that scans mRNAs for start codons. After start codon detection, eIF2γ hydrolyzes its GTP and translation initiates. For eIF2 reactivation, guanosine diphosphate (GDP) is replaced by GTP upon catalysis by a dedicated guanine nucleotide exchange factor (GEF), eIF2B.

eIF2 and eIF2B control translation initiation. Stress-responsive kinases phosphorylate eIF2α at the conserved residue Ser^{51}, transforming eIF2 from substrate into a competitive GEF inhibitor. Phosphoregulation of eIF2 is known as the integrated stress response (ISR) (*1*). Once activated, the ISR reduces overall protein synthesis while enhancing translation of a small subset of mRNAs in response to cellular threats, including protein misfolding, infection, inflammation, and starvation (*1*–*3*).

eIF2B comprises two copies each of an α, β, γ, δ, and ε subunit that assemble into a two-fold symmetric heterodecamer (*4*, *5*). The eIF2Bε subunit contains the enzyme's catalytic center and associates closely with eIF2Bγ. Two copies each of the eIF2Bβ and eIF2Bδ subunits form the complex's core, bridged by two eIF2Bα subunits across the symmetry interface (*4*, *6*). Genetic and biochemical studies have identified residues responsible for eIF2B's catalytic activity and have suggested how eIF2 binding to eIF2B may differ after eIF2α Ser^{51} phosphorylation (*4*, *7*–*10*). Yet it has remained unknown how eIF2 recognizes eIF2B, how eIF2B catalyzes nucleotide exchange, or how eIF2 transforms from a substrate to a high-affinity inhibitor of eIF2B after its phosphorylation.

A potent small-molecule, drug-like inhibitor of the integrated stress response, ISRIB, allays the effects of eIF2α phosphorylation by activating eIF2B (*11*–*13*). Upon adding ISRIB, cells undergoing the ISR resume translation (*12*, *13*). When administered to rodents, ISRIB enhances cognition and ameliorates cognitive deficits caused by traumatic brain injury (*14*) and prion-induced neurodegeneration (*15*). Furthermore, eIF2B activation rescues cognitive and motor function in mouse models of leukoencephalopathy with vanishing white matter disease (VWMD), a fatal familial disorder associated with mutations spread over all eIF2B subunits (*16*).

ISRIB bridges the symmetric interface of two eIF2B subcomplexes to enhance the formation of the decameric eIF2B holoenzyme (*17*, *18*), enhancing available GEF activity by promoting higher-order assembly of the eIF2B decamer. However, it has remained an enigma why decameric eIF2B would be more active than its unassembled subcomplexes. To explore this question, we determined structures of eIF2B bound with both its substrate, eIF2 (α,β,γ), and its inhibitor, eIF2α•P.

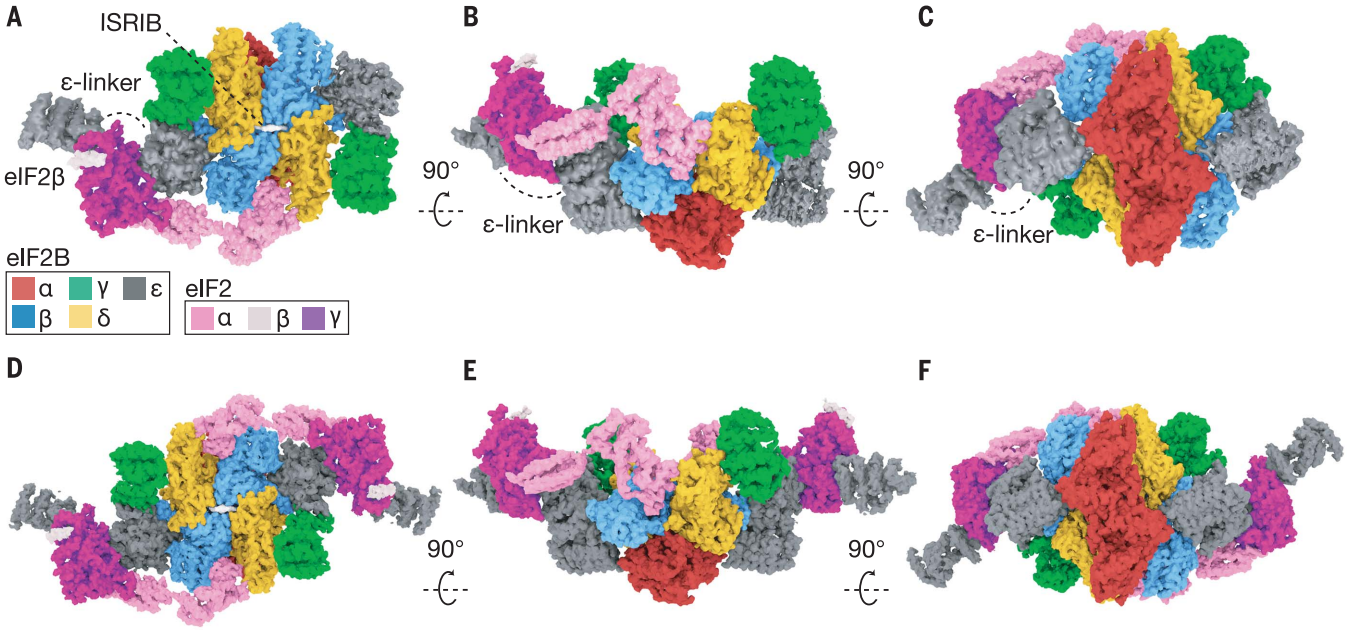

Fig. 1. eIF2B heterodecamer bound to one or two eIF2 heterotrimers. (**A** to **C**) Orthogonal views of a single elongated eIF2 heterotrimer bound to ISRIB-stabilized eIF2B decamers. ISRIB density is rendered in white. (**D** to **F**) Orthogonal views of a pair of elongated eIF2 heterotrimers bound to ISRIB-stabilized eIF2B decamers. ISRIB density is rendered in white.

We coexpressed all five subunits of human eIF2B in *Escherichia coli* and all three subunits of human eIF2 in *Saccharomyces cerevisiae* (fig. S1, A and B). The yeast expression strain lacked *GCN2*, an eIF2 kinase, to ensure expression of homogeneously nonphosphorylated eIF2 (*19*). We incubated ISRIB and purified eIF2 at concentrations near the Michaelis constant of the nucleotide exchange reaction [K_m = ~1.5 μM (*17*)] and added an inter-amine cross-linker to stabilize complexes before sample vitrification and cryo–electron microscopy (cryo-EM) analysis (fig. S2, A to C). We resolved two structures: eIF2B bound asymmetrically to a single eIF2 trimer and eIF2B bound symmetrically to two eIF2 trimers (Fig. 1, figs. S3A, S4, and S5, and tables S1 to S3).

Snaking across the surface of eIF2B, we observed density consistent in size and shape with eIF2 subunits and the previously unresolved eIF2Bε HEAT domain. Comparison with homologous structures of eIF2α and eIF2γ revealed that the assembled eIF2•eIF2B complex retained similarity to the structures of these individually analyzed domains (*20*–*22*) (Fig. 2 and fig. S6). We resolved only a single helix of eIF2β (Fig. 1, A and D, and Fig. 2A), consistent with other studies (*20*, *21*). In both reconstructions, all five subunits of eIF2B can be superimposed on previously determined structures lacking eIF2 [root mean square deviation (RMSD) ≈ 0.6 Å] (*17*). Thus, eIF2B retained its overall arrangement when bound to one or two eIF2s (Fig. 1), indicating that eIF2 binds via equivalent modes to both sides of a static eIF2B scaffold with no allostery in eIF2B upon eIF2 engagement. This is consistent with noncooperative kinetics reported for nucleotide exchange by eIF2B decamers (*17*).

Bound to eIF2B, eIF2 adopted an extended 150 Å conformation (Figs. 1 and 2A) with eIF2's central nucleotide-binding γ subunit flanked by its α and β subunits at its opposing ends. eIF2γ contains classical GTP-binding motifs, including the nucleobase-binding G4 motif, the phosphate-binding P-loop, and switch helices 1 and 2. eIF2B recognizes eIF2 via coincident binding of both eIF2α and eIF2γ. Binding to both eIF2 subunits involves bipartite elements of eIF2B (Fig. 1 and Fig. 2, A to C).

First, bipartite recognition of eIF2γ involves two domains of eIF2Bε that function together to splay open the nucleotide-binding site. Our nucleotide-free cryo-EM model is similar to the γ subunit of GTP-bound aIF2 from *Sulfolobus solfataricus* (*23*) (Fig. 2, D and E; average RMSD ≈ 2.3 Å). However, surrounding the GTP-binding pocket, the structures diverged considerably, with the P-loop in eIF2B•eIF2 partially occluding the nucleotide-binding site (RMSD ≈ 12 Å). Prior work implicated the HEAT domain in catalysis (*23*–*26*). In agreement with those findings, eIF2γ interacts with the HEAT domain, including a partially hydrophobic surface that includes eIF2Bε Tyr^{583} (Fig. 2C). On the opposing side of the nucleotide-binding pocket, the central core of eIF2Bε engaged with an open-loop conformation of switch 1. This change appears to be due to electrostatic interactions between eIF2γ Arg^{75} in switch 1 and Gln^{258} and Asp^{262} in eIF2Bε (Fig. 2B). Thus, both eIF2Bε's HEAT domain and core collaborate to open the nucleotide-binding site (Fig. 2, B to D).

The second example of bipartite recognition concerns eIF2α binding in the cleft between eIF2Bβ and eIF2Bδ′ (δ′ denotes the δ subunit

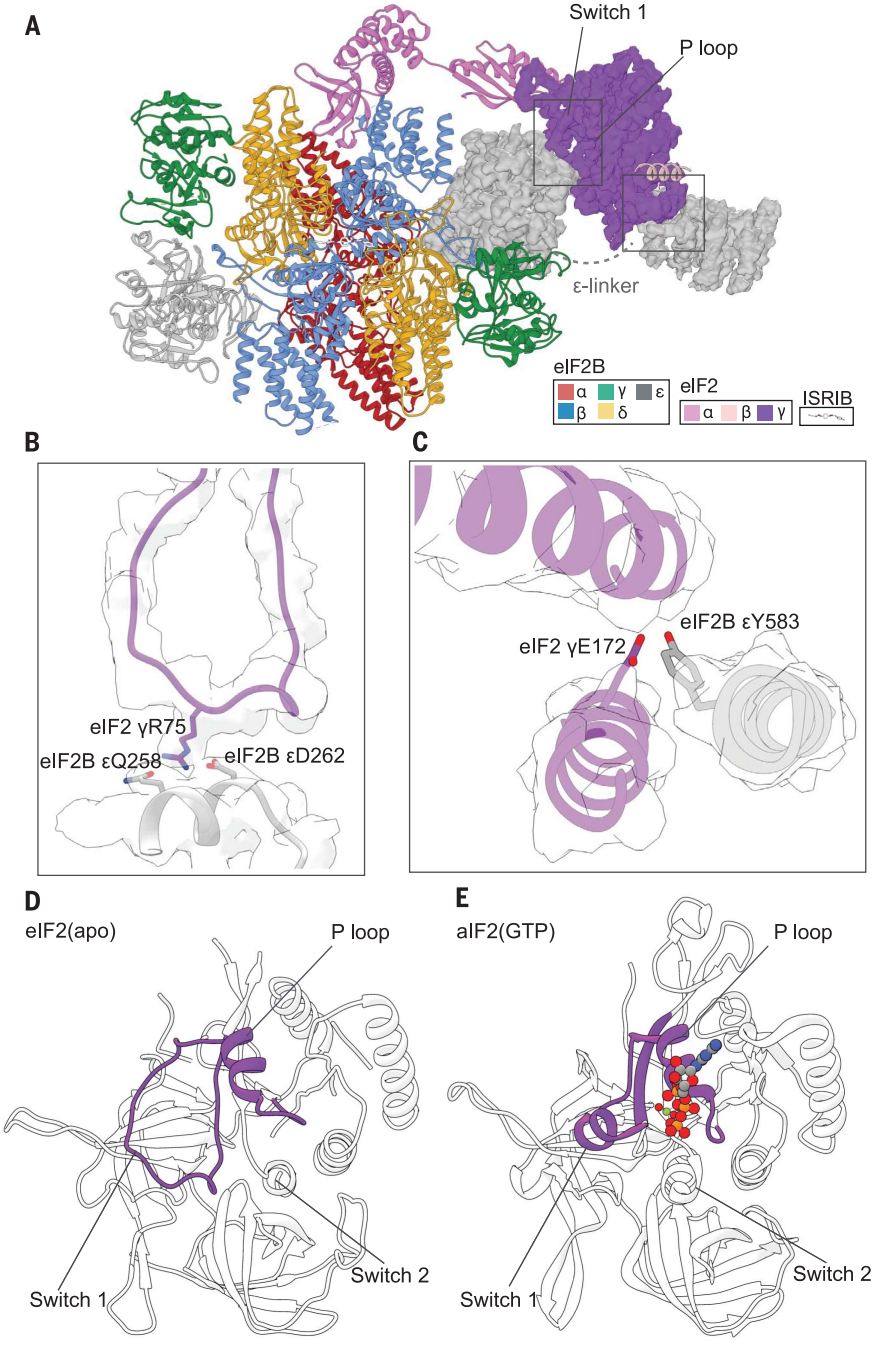

Fig. 2. The bipartite basis of guanine nucleotide exchange by eIF2B. (**A**) Structural model of a single eIF2 heterotrimer bound to the eIF2B decamer, emphasizing the cryo-EM density for eIF2γ and its interactions with eIF2Bε. (**B**) Switch 1 of eIF2γ stabilized as an open loop due to interactions between R75 eIF2γ and Q258 and D262 of eIF2Bε. (**C**) Y583 from the HEAT domain of eIF2Bε (one helix shown) contacting eIF2γ E172. (**D** and **E**) Comparison of the open, nucleotide-free state of eIF2 reported here (D) and an aIF2 structure bound to GTP (PDB: 4RCY) (E). Amino acid abbreviations: D, Asp; E, Glu; Q, Gln; R, Arg; Y, Tyr.

[1]Department of Biochemistry and Biophysics, University of California, San Francisco, CA, USA. [2]Howard Hughes Medical Institute, University of California, San Francisco, CA, USA. [3]Centre for Integrative Biology, Department of Integrated Structural Biology, IGBMC, CNRS, Inserm, Université de Strasbourg, 67404 Illkirch, France. [4]Chan Zuckerberg Biohub, San Francisco, CA, USA.
*These authors contributed equally to this work.
†Corresponding author. Email: peter@walterlab.ucsf.edu (P.W.); adam.frost@ucsf.edu (A.F.)

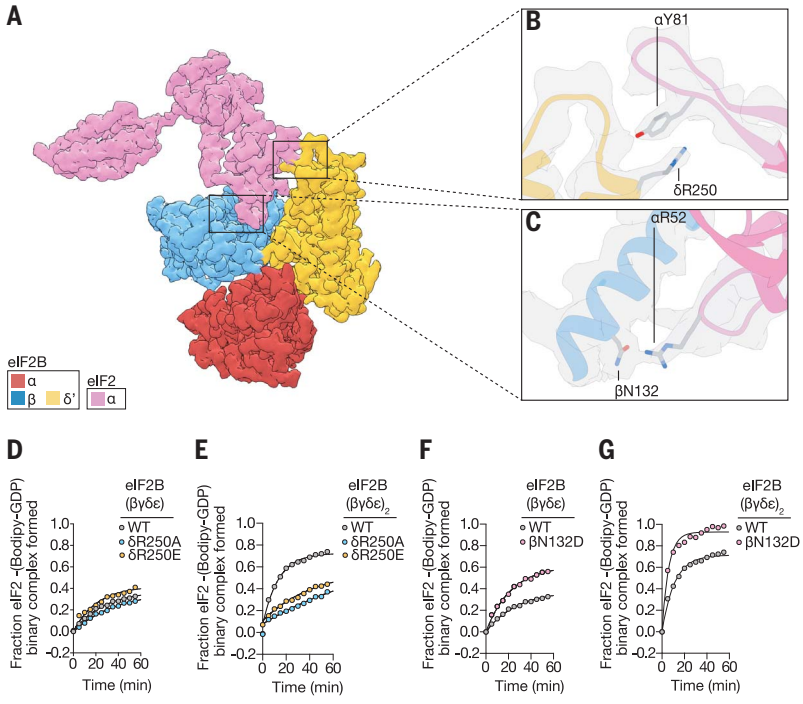

Fig. 3. The bipartite basis of eIF2α recognition and assembly-stimulated activity. (**A**) Cryo-EM density for eIF2α bound to the regulatory subcomplex (α, β, δ, or RSC) of eIF2B. (**B**) Density and zoom-in detail of a cation-π interaction between eIF2Bδ and eIF2α. (**C**) Polar interactions between eIF2Bβ and the S-loop of eIF2α. (**D** and **F**) GEF activity of wild-type versus mutated eIF2B (βγδε) tetramers measured by BODIPY-labeled GDP fluorescence unquenching. (**E** and **G**) ISRIB-stabilized eIF2B $(\beta\gamma\delta\varepsilon)_2$ octamers measured by BODIPY-labeled GDP fluorescence unquenching. A, Ala; N, Asn.

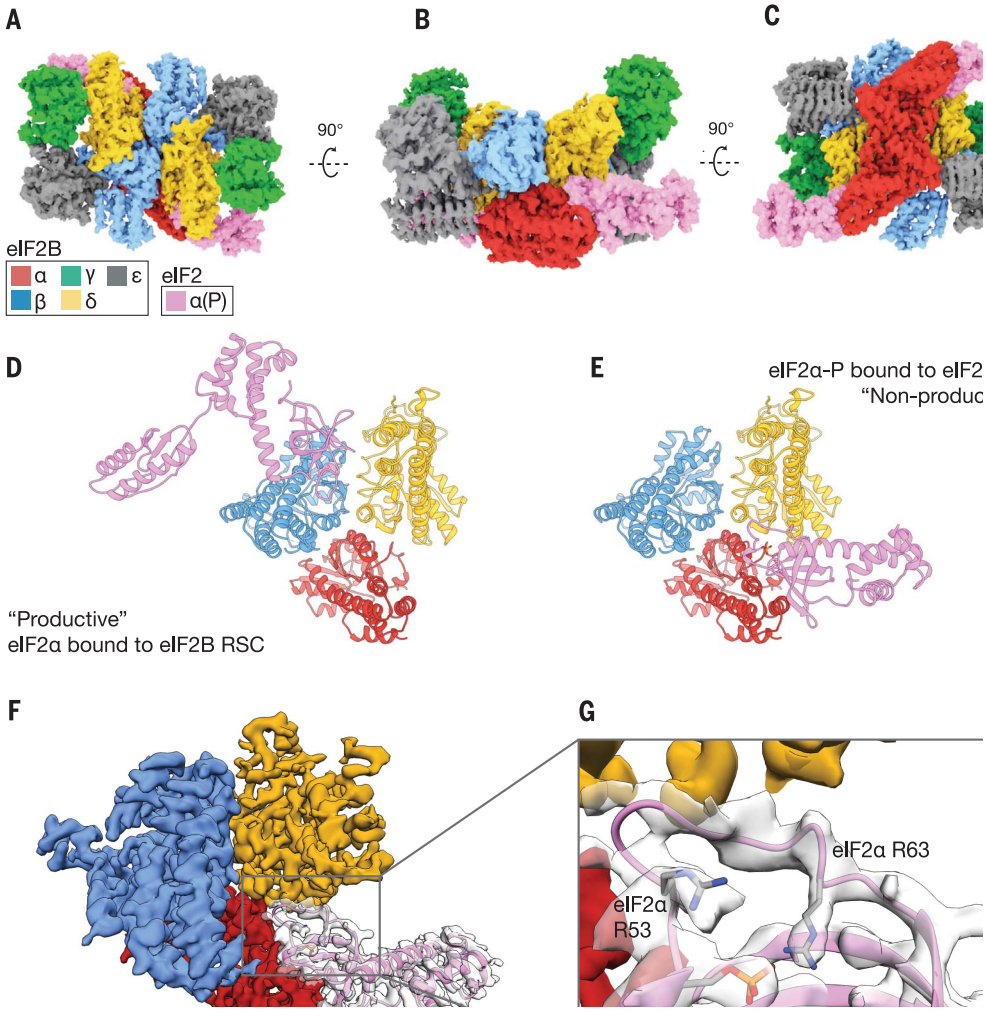

Fig. 4. The structural basis of phosphoregulation by the ISR. (**A** to **C**) Orthogonal views of a pair of Ser[51]-phosphorylated eIF2α subunits bound to the eIF2B decamer. (**D**) The productive binding mode of nonphosphorylated eIF2α. (**E**) The nonproductive and nonoverlapping binding mode of phosphorylated eIF2α. (**F**) Cryo-EM density of phosphorylated eIF2α bound to the regulatory subcomplex (α, β, δ) of eIF2B. (**G**) Zoom-in of the S-Loop cryo-EM density and model, placing the Ser[51] phosphate moiety near eIF2α Arg[53] and Arg[63].

from the opposing tetramer) (Figs. 1 to 3). Notably, this binding site only exists when two tetramers of eIF2B (βγδε) associate to form the symmetry interface in octameric eIF2B $(\beta\gamma\delta\varepsilon)_2$. eIF2α contains two structured domains separated by a flexible linker (Figs. 1 and 2 and fig. S6). The N terminus consists of an OB-fold, common in tRNA-binding proteins (*20*). The OB-fold is further elaborated with a positively charged loop (the S-loop), while the C-terminal αβ-fold connects eIF2α to eIF2γ. The S-loop harbors Ser^{51} and is responsible for all of the resolvable contacts between eIF2α and eIF2B's β subunit (Fig. 3A). Prior work implicated a conserved "^{79}KGYID^{83}" (Lys^{79}-Gly^{80}-Tyr^{81}-Ile^{82}-Asp^{83}) motif in eIF2α as being important for eIF2B binding (*10*). Of note, an interaction between Tyr^{81} was well resolved adjacent to the equally prominent Arg^{250} on eIF2Bδ′ (Fig. 3B). When we mutated Arg^{250} to either alanine (R250A) or glutamate (R250E), neither mutation affected the residual GEF activity displayed by dissociated tetramers (Fig. 3D; R250A k_{obs} = 0.013 min^{-1}, R250E k_{obs} = 0.023 min^{-1}, wild-type k_{obs} = 0.016 min^{-1}), whereas both mutants diminished the GEF activity of the ISRIB-stabilized eIF2B octamer when compared to the wild type (Fig. 3E; R250A k_{obs} = 0.012 min^{-1}, R250E k_{obs} = 0.017 min^{-1},wild-type k_{obs} = 0.063 min^{-1}). This is consistent with the notion that unphosphorylated eIF2α interacts with the trans tetramer only upon assembly of octameric or decameric eIF2B across its symmetry interface.

On the cis tetramer, eIF2α's positively charged S-loop binds negatively charged and polar residues along the exposed surface of eIF2Bβ. This binding site is consistent with yeast studies suggesting that mutations in this site compromise eIF2 binding (*7*). Examination of the structure identified a potential hydrogen bond between eIF2Bβ Asn^{132} and eIF2α Arg^{52} (Fig. 3C). We substituted Asn^{132} with aspartate (N132D), anticipating that the introduced charge complementarity would enhance binding to eIF2α Arg^{52}. When compared to wild-type eIF2B tetramers, eIF2B-βN132D tetramers and ISRIB-stabilized octamers indeed proved to be gain-of-function mutations, exhibiting enhanced GEF activity by a factor of ~2 [Fig. 3, F and G, and fig. S1D; eIF2B (βγδε) βN132D k_{obs} = 0.044 min^{-1}, eIF2B $(\beta\gamma\delta\varepsilon)_2$ βN132D k_{obs} = 0.169 min^{-1}]. This is consistent with eIF2B tetramers possessing reduced activity relative to assembled octameric or decameric holo-eIF2B. eIF2α binding in the cleft between tetramers further supports the notion that ISRIB enhances eIF2B's GEF activity by promoting higher-order assembly.

To understand how eIF2α phosphorylation on Ser^{51} transforms eIF2 from substrate to inhibitor, we coexpressed the isolated eIF2α subunit in *E. coli* with the kinase domain of PERK (double-stranded RNA–activated protein kinase-like ER kinase), an eIF2 kinase (fig. S1C). We incubated preassembled eIF2B decamers with an excess of eIF2α-P, followed by cross-linking and vitrification. Reconstruction of the eIF2B decamer adorned with two copies of eIF2α-P (Fig. 4A, figs. S7 and S8, and tables S1 to S3) revealed eIF2α-P bridging the interface between eIF2Bδ and eIF2Bα (Fig. 4A). Intriguingly, we observed no overlap between the binding sites of nonphosphorylated eIF2α described above and eIF2α-P (Fig. 4, B and C).

Density for both eIF2α Ser^{51}-P and two arginines positioned ~4 Å away, eIF2α Arg^{53} and Arg^{63}, were well resolved and suggestive of an electrostatic coordination responsible for phosphorylation-induced refolding of the S-loop (Fig. 4, F and G, fig. S8, and movie S1), as initially observed by Kashiwagi *et al.* (*27*). The phosphorylation-induced rearrangement also positions hydrophobic residues on eIF2α for potential interactions with hydrophobic residues on eIF2B (including eIF2α Ile^{55}, Ile^{58}, and Leu^{61} and eIF2Bδ Leu^{314}, Ala^{315}, Ala^{318}, and Phe^{322}).

This structural model agrees with analyses in yeast and mammalian systems. eIF2Bα is dispensable for viability in yeast, yet eIF2Bα deletion impairs phospho-inhibition of eIF2B, consistent with the subunit's role in binding eIF2α-P (*28*). Point mutations with identical phenotypes cluster at the interface between eIF2Bα and eIF2Bδ (e.g., eIF2Bα Phe^{239} and eIF2Bδ Met^{506} and Pro^{508}) (*29*, *30*). eIF2Bδ Leu^{314} complements the hydrophobic surface of the eIF2α S-loop that is exposed upon refolding, and mutation of Leu to Gln at the equivalent position in *S. cerevisiae*, L381Q, impairs the ISR in yeast (*29*). These data validate the phosphorylation-induced refolding and relocation of eIF2α-P observed here.

Our analyses reveal the mechanistic basis of eIF2B's nucleotide exchange activity and suggest how phosphorylation converts eIF2 from substrate to inhibitor. The nonphosphorylated form of eIF2 binds to a composite surface created only in the assembled decamer, allowing both the core and the flexibly attached HEAT domain of eIF2Bε to engage its target in concert for enhanced GEF activity.

By contrast, eIF2α-P adopts a new conformation and suggests how the S-loop may become incompatible for binding to the site where nonphosphorylated eIF2α binds as a substrate (movie S1). Phosphorylation thus enables a distinct binding mode on the opposite side of eIF2B where eIF2α-P lies exiled at the interface of eIF2Bα and eIF2Bδ. In eIF2α•P, the rearrangement of the S-loop derives from an intramolecular electrostatic interaction between Arg^{63} and Arg^{53} and the phosphate, which also exposes a hydrophobic surface upon phosphorylation-induced refolding. We surmise that this new binding mode is nonproductive for nucleotide exchange on eIF2-P and sequesters the catalytic domains into an inhibited state that prevents the catalytic moieties of eIF2Bε from properly engaging in productive nucleotide exchange.

REFERENCES AND NOTES

1. H. P. Harding *et al.*, *Mol. Cell* **11**, 619–633 (2003).
2. L. R. Palam, T. D. Baird, R. C. Wek, *J. Biol. Chem.* **286**, 10939–10949 (2011).
3. K. M. Vattem, R. C. Wek, *Proc. Natl. Acad. Sci. U.S.A.* **101**, 11269–11274 (2004).
4. K. Kashiwagi *et al.*, *Nature* **531**, 122–125 (2016).
5. Y. Gordiyenko *et al.*, *Nat. Commun.* **5**, 3902 (2014).
6. B. Kuhle, N. K. Eulig, R. Ficner, *Nucleic Acids Res.* **43**, 9994–10014 (2015).
7. K. Dev *et al.*, *Mol. Cell. Biol.* **30**, 5218–5233 (2010).
8. G. D. Pavitt, K. V. Ramaiah, S. R. Kimball, A. G. Hinnebusch, *Genes Dev.* **12**, 514–526 (1998).
9. S. R. Kimball, J. R. Fabian, G. D. Pavitt, A. G. Hinnebusch, L. S. Jefferson, *J. Biol. Chem.* **273**, 12841–12845 (1998).
10. T. Krishnamoorthy, G. D. Pavitt, F. Zhang, T. E. Dever, A. G. Hinnebusch, *Mol. Cell. Biol.* **21**, 5018–5030 (2001).
11. C. Sidrauski *et al.*, *eLife* **2**, e00498 (2013).
12. C. Sidrauski *et al.*, *eLife* **4**, e07314 (2015).
13. Y. Sekine *et al.*, *Science* **348**, 1027–1030 (2015).
14. A. Chou *et al.*, *Proc. Natl. Acad. Sci. U.S.A.* **114**, E6420–E6426 (2017).
15. M. Halliday *et al.*, *Cell Death Dis.* **6**, e1672 (2015).
16. Y. L. Wong *et al.*, *eLife* **7**, e32733 (2018).
17. J. C. Tsai *et al.*, *Science* **359**, eaaq0939 (2018).
18. A. F. Zyryanova *et al.*, *Science* **359**, 1533–1536 (2018).
19. R. A. de Almeida *et al.*, *PLOS ONE* **8**, e53958 (2013).
20. T. Ito, A. Marintchev, G. Wagner, *Structure* **12**, 1693–1704 (2004).
21. S. Dhaliwal, D. W. Hoffman, *J. Mol. Biol.* **334**, 187–195 (2003).
22. B. Eliseev *et al.*, *Nucleic Acids Res.* **46**, 2678–2689 (2018).
23. E. Dubiez, A. Aleksandrov, C. Lazennec-Schurdevin, Y. Mechulam, E. Schmitt, *Nucleic Acids Res.* **43**, 2946–2957 (2015).
24. V. Beilsten-Edmands *et al.*, *Cell Discov.* **1**, 15020 (2015).
25. T. Boesen, S. S. Mohammad, G. D. Pavitt, G. R. Andersen, *J. Biol. Chem.* **279**, 10584–10592 (2004).
26. J. Wei *et al.*, *Protein Cell* **1**, 595–603 (2010).
27. K. Kashiwagi *et al.*, *Science* **364**, 495–499 (2019).
28. R. Elsby *et al.*, *J. Virol.* **85**, 9716–9725 (2011).
29. G. D. Pavitt, W. Yang, A. G. Hinnebusch, *Mol. Cell. Biol.* **17**, 1298–1313 (1997).
30. C. R. Vazquez de Aldana, A. G. Hinnebusch, *Mol. Cell. Biol.* **14**, 3208–3222 (1994).

ACKNOWLEDGMENTS

We thank E. Pavolcak, J. Peschek, E. Karagöz, M. Boone, V. Belyy, G. Narlikar, R. Vale, and members of the Walter and Frost laboratories; D. Asarnow for creating PyEM; E. Green for help with cisTEM; P. Thomas for computational support; A. Melo for help with Blender; the UCSF Center for Advanced CryoEM, which is supported by NIH grants S10OD020054 and 1S10OD021741 and the Howard Hughes Medical Institute (HHMI); Z. Yu and H. Chou of the CryoEM Facility at the HHMI Janelia Research Campus (NIH grant 1S10OD021596-01) for computational support; and G. Pavitt for the GP6452 yeast strain used in the purification of eIF2. A Titan X Pascal used for this research was donated by the NVIDIA Corporation. **Funding:** Supported by an HHMI Faculty Scholar grant (A.F.) and by Calico Life Sciences LLC, the Rogers Family Foundation, the Weill Foundation, and HHMI (P.W.). L.R.K. was supported by a graduate research fellowship from the N.S.F. A.F. is a Chan Zuckerberg Biohub Investigator, and P.W. is an Investigator of HHMI. **Author contributions:** Conception and design, analysis and interpretation of data: L.R.K., A.A.A., H.C.N., P.W., and A.F.; acquisition of data: L.R.K., A.A.A., A.G.M.; writing (original draft): L.R.K., A.A.A., P.W., and A.F.; writing (review and editing): L.R.K., A.A.A., H.C.N., A.G.M., C.J.K., L.A.M., J.C.T., L.E.M.-V., A.F., and P.W. **Competing interests:** P.W. is an inventor on U.S. Patent 9708247 held by the Regents of the University of California that describes ISRIB and its analogs. Rights to the invention have been licensed by UCSF to Calico. **Data and materials availability:** All data needed to evaluate the conclusions in the paper are present in the paper and/or the supplementary materials, and the structural data are available in public databases. All of the raw cryo-EM data are also available upon request. The GP6452 yeast strain is available under a material transfer agreement with the University of Manchester. Accession numbers for the human eIF2•eIF2B structures are as follows: EMD-0649, EMD-0651, EMD-0664 (density maps; Electron Microscopy Data Bank) and PDB-6O81, PDB-6O85, PDB-6O9Z (coordinates of atomic models; Protein Data Bank).

SUPPLEMENTARY MATERIALS

science.sciencemag.org/content/364/6439/491/suppl/DC1
Materials and Methods
Figs. S1 to S7
Tables S1 to S3
Movie S1
References (*31*–*42*)

21 December 2018; accepted 8 April 2019
10.1126/science.aaw2922

Science

eIF2B-catalyzed nucleotide exchange and phosphoregulation by the integrated stress response

Lillian R. Kenner, Aditya A. Anand, Henry C. Nguyen, Alexander G. Myasnikov, Carolin J. Klose, Lea A. McGeever, Jordan C. Tsai, Lakshmi E. Miller-Vedam, Peter Walter and Adam Frost

Science **364** (6439), 491-495.
DOI: 10.1126/science.aaw2922

Integrated stress response on the brain

During translation, regulation of protein synthesis by phosphorylation of eukaryotic translation initiation factor 2 (eIF2) is a common consequence of diverse stress stimuli, which leads to reprogramming of gene expression. This process, known as the integrated stress response, is one of the most fundamental mechanisms of translational control conserved throughout eukaryotes. It is also a promising therapeutic target in neurodegenerative diseases and traumatic brain injury. Kashiwagi *et al.* report the cryo–electron microscopy and crystal structures and Kenner *et al.* report the cryo–electron microscopy structure of the guanine nucleotide exchange factor eIF2B in complex with eIF2 or phosphorylated eIF2. The structures of the eIF2 •eIF2B complex reveal that the single phosphorylation modification on eIF2 changes how eIF2 binds to eIF2B and locks this enzyme into an inhibited complex.

Science, this issue p. 495, p. 491